Vol 16 No 8, August 2007
1009-1963/2007/16(08)/2319-06

Chinese Physics

© 2007 Chin. Phys. Soc.
and IOP Publishing Ltd

Influence of tube voltage and current on in-line phase contrast imaging using a microfocus x-ray source*

Li Chen(李 晨)†, Li Zheng(李 政),
Yu Ai-Min(禹爱民), and Li Cheng-Quan(黎成权)

Department of Engineering Physics, Tsinghua University, Beijing 100084, *China*

(Received 17 October 2006; revised manuscript received 21 December 2006)

In-line x-ray phase contrast imaging has attracted much attention due to two major advantages: its effectiveness in imaging weakly absorbing materials, and the simplicity of its facilities. In this paper a comprehensive theory based on Wigner distribution developed by Wu and Liu [Med. Phys. 31 2378-2384 (2004)] is reviewed. The influence of x-ray source and detector on the image is discussed. Experiments using a microfocus x-ray source and a CCD detector are conducted, which show the role of two key factors on imaging: the tube voltage and tube current. High tube current and moderate tube voltage are suggested for imaging.

Keywords: x-ray, in-line phase contrast imaging, Wigner distribution
PACC: 0785, 4230K

1. Introduction

Since Roentgen discovered x-ray and performed the first x-ray imaging in 1895, x-ray imaging has been widely-used in clinical and industrial nondestructive diagnosis, as well as in biological and material research. However, x-ray imaging has always been based on contrast produced by objects' absorption attenuation and this has remained unchanged for over 100 years. When it comes to weakly absorbing materials such as soft tissues, they produce little absorption contrast so that conventional x-ray imaging can hardly detect sufficient information of their insides.

However, as x-ray is an electromagnetic wave, its interaction with object produces not only intensity change, but also phase changes. The amount of both intensity and phase changes is determined by the object's refractive index, which is given by

$$n = 1 - \delta + \mathrm{i}\beta, \tag{1}$$

where δ is responsible for phase changes, and β is responsible for absorption. For light elements, δ is about 1000 times larger than β.[1] Thus for soft tissues mainly composed of light elements, the phase shift of x-ray passing through it is much easier to detect than the intensity change. In the mid-1990s, several methods of phase contrast x-ray imaging were developed. There are three major methods: interferometric method, diffraction enhanced imaging (DEI) and in-line phase contrast imaging. The interferometric method, brought forward by Momose,[2] uses x-ray interferometers to get φ image, where φ is the local phase of the specimen. The DEI method, first performed by Davis *et al*[3] and Ingral and Beliaevskaya,[4] utilizes one or more crystals to get $\nabla\varphi$ image. Compared with the two former methods, the in-line method has the simplest light path for it requires no additional optical component except an x-ray source, an object stage, and an x-ray detector. A microfocus x-ray source is suitable for in-line method. Thus, in-line phase contrast imaging is small in size, cheap in cost, and convenient to perform, and has great potential for future application.

Pogany *et al*'s theory[5] of describing in-line phase contrast imaging is widely used. This theory is based on the paraxial Fresnel–Kirchhoff diffraction theory for spatially coherent x-ray sources, but it is not suitable for microfocus x-ray sources because they are not spatially coherent and the impact of the detector is not taken into account. To overcome this limitation, Zhu *et al*[6] developed a theory that can describe the influence of polychroism of radiation on imaging. In 2004, Wu and Liu publicized a more comprehensive theory,[7] which can deal with partially coherent x-ray,

*Project supported by the National Natural Science Foundation of China (Grant No 10475044).
†Corresponding author. E-mail: lichen19853@gmail.com

and the detector's impact is taken into consideration. In this paper, the new theory is briefly reviewed and the influence of x-ray source and detector is discussed. Experiments are carried out to show the role of tube current and voltage in the imaging.

2. Theory of in-line phase contrast imaging

In order to incorporate the x-ray source's partial coherency, new theory uses Wigner distribution function (WDF). Wigner distribution function was originally introduced by Wigner[8] in 1932 to describe mechanical phenomena in a phase space. It was introduced into optics to describe partially coherent light by Bastiaans[9] in 1978. It is written as

$$W(\boldsymbol{r},\boldsymbol{u};z) = \int J(\boldsymbol{r}+\boldsymbol{q}/2,\boldsymbol{r}-\boldsymbol{q}/2;z) \times \exp(-\mathrm{i}2\pi\boldsymbol{q}\cdot\boldsymbol{u})\mathrm{d}\boldsymbol{q}, \quad (2)$$

where $J(\boldsymbol{r}_1,\boldsymbol{r}_2;z)$ is the mutual intensity at distance z from the source plane, $\boldsymbol{r}$ and $\boldsymbol{u}$ represent a 2D space vector and a 2D frequency vector respectively. Thus WDF describes the light in space and spatial frequency simultaneously.

A schematic sketch of the in-line phase contrast imaging is shown in Fig.1. The object is illuminated

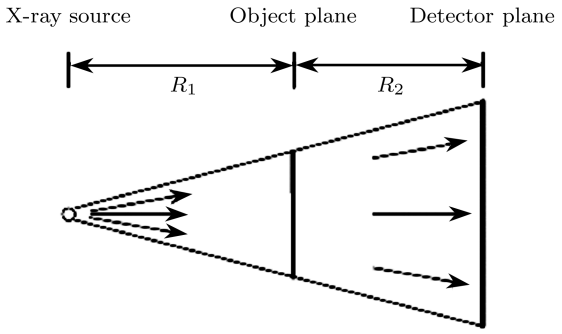


Fig.1. Schematic sketch of in-line phase contrast imaging.

by a spherical x-ray source. The object plane is parallel to the image plane, and specimen can be viewed as thin objects for resolution as high as 10 micron for x-ray photon energies higher than 10 keV and lower than 150 keV.[7] The distance between the x-ray source and the object plane is R_1, and the distance from the object plane to the image plane is R_2.

Using the properties of WDF,[10] we can write the x-ray intensity at the detector plane as

$$I(\boldsymbol{r};R_1+R_2) = \int W(\boldsymbol{r},\boldsymbol{u};R_1+R_2)\mathrm{d}\boldsymbol{u} = \int W(\boldsymbol{r}-\lambda R_2\boldsymbol{u},\boldsymbol{u};R_1)\mathrm{d}\boldsymbol{u}. \quad (3)$$

Let $T(\boldsymbol{r})$ be the 2D transfer function of the object which can be written as

$$T(\boldsymbol{r}) = A(\boldsymbol{r})\mathrm{e}^{\mathrm{i}\phi(\boldsymbol{r})} = \exp\left[\mathrm{i}\phi(\boldsymbol{r}) - \frac{\mu_p(\boldsymbol{r})}{2}\right], \quad (4)$$

where $\phi(\boldsymbol{r})$ and $\mu_p(\boldsymbol{r})$ denote the integration of the object phase and linear attenuation coefficient along the direction of x-ray propagation respectively.

Substituting Eq.(4) into Eq.(3), and letting $\widetilde{I}(\boldsymbol{u};R_1+R_2)$ be the Fourier transform of $I(\boldsymbol{r};R_1+R_2)$, we found that

$$\tilde{I}(\boldsymbol{u};R_1+R_2) = \int J(\boldsymbol{s}+\lambda R_2\boldsymbol{u}/2,\boldsymbol{s}-\lambda R_2\boldsymbol{u}/2) \times T(\boldsymbol{s}+\lambda R_2\boldsymbol{u}/2)T^*(\boldsymbol{s}-\lambda R_2\boldsymbol{u}/2) \times \mathrm{e}^{\mathrm{i}2\pi\boldsymbol{s}u}\mathrm{d}\boldsymbol{s}. \quad (5)$$

Considering that the size of the x-ray source is much smaller than R_1, we can treat the incident x-ray intensity at the object plane as constant intensity. Thus, we have

$$J(\boldsymbol{s}_1,\boldsymbol{s}_2) = \sqrt{I_{\mathrm{in}}(\boldsymbol{s}_1)I_{\mathrm{in}}(\boldsymbol{s}_2)}\mu_{\mathrm{in}}(\boldsymbol{s}_1,\boldsymbol{s}_2) \approx I_{\mathrm{in}}\mu_{\mathrm{in}}(\boldsymbol{s}_1,\boldsymbol{s}_2). \quad (6)$$

According to the Cittert–Zernike theorem,[11]

$$\mu(\boldsymbol{s}_1,\boldsymbol{s}_2) = \widetilde{\mu}(\boldsymbol{s}_1,\boldsymbol{s}_2)\exp\left(\mathrm{i}\frac{\boldsymbol{s}_1^2-\boldsymbol{s}_2^2}{\lambda R_1}\right), \quad (7)$$

where the expression $\widetilde{\mu}(\boldsymbol{s}_1,\boldsymbol{s}_2)$ is called the reduced complex degree of coherence (RCDC),[7] we get

$$\tilde{I}\left(\frac{\boldsymbol{u}}{M};R_1+R_2\right) = I_{\mathrm{in}}\tilde{\mu}\left(\frac{\lambda R_2\boldsymbol{u}}{2M}\right)\int T\left(\boldsymbol{s}+\frac{\lambda R_2\boldsymbol{u}}{2M}\right)T^*\left(\boldsymbol{s}-\frac{\lambda R_2\boldsymbol{u}}{2M}\right)\mathrm{e}^{\mathrm{i}2\pi\boldsymbol{s}u}\mathrm{d}\boldsymbol{s}. \quad (8)$$

In application, we always have $|\lambda R_2\boldsymbol{u}/2M| \ll 1\,\mu$m.[12] Based on this fact, we finally get the x-ray intensity

at the image plane:

$$I(\boldsymbol{r};R_1+R_2)=\left(\frac{I_{\rm in}}{M^2}\right)\mathrm{FT}^{-1}\left(\tilde{\mu}_{\rm in}\left(\frac{\lambda R_2\boldsymbol{u}}{M}\right)\cdot\mathrm{OTF}_{\rm det}\left(\frac{\boldsymbol{u}}{M}\right)\right)\otimes\left\{A_0^2\left(\frac{\boldsymbol{r}}{M}\right)-\left(\frac{\lambda R_2}{2\pi M}\right)\nabla(A_0^2\nabla\phi\left(\frac{\boldsymbol{r}}{M}\right)\right\},\quad(9)$$

where FT^{-1} denotes inverse Fourier transform, and $\mathrm{OTF}_{\rm det}(\boldsymbol{u})$ is the detector's frequency response at $\boldsymbol{u}$. As long as the spatial frequency is smaller than the Nyquest frequency, Eq.(9) holds. This result holds for partially coherent x-ray sources such as microfocus x-ray sources, and it shows the impact of the detector to in-line phase contrast imaging. In the following chapters, we will utilize this result to analyse the influence of detector and x-ray source.

3. The influence of x-ray source and detector

In this work, we will focus our discussion on CCD detectors and microfocus x-ray sources, which are the most frequently used detectors and light sources in in-line phase contrast imaging.

Reviewing Eq.(9), we find that the first part $\left(\frac{I_{\rm in}}{M^2}\right)$ determines the overall intensity of the image, the second part $\mathrm{FT}^{-1}\left(\tilde{\mu}_{\rm in}\left(\frac{\lambda R_2\boldsymbol{u}}{M}\right)\cdot\mathrm{OTF}_{\rm det}\left(\frac{\boldsymbol{u}}{M}\right)\right)$ serves as a filter to the final image, and it is the third part $\left\{A_0^2\left(\frac{\boldsymbol{r}}{M}\right)-\left(\frac{\lambda R_2}{2\pi M}\right)\nabla\left(A_0^2\nabla\phi\left(\frac{\boldsymbol{r}}{M}\right)\right)\right\}$ that determines the contrast of the image.

Firstly, let us consider the influence of x-ray photon energy, which can be denoted by the x-ray wave length λ and is embodied in the part $\left\{A_0^2\left(\frac{\boldsymbol{r}}{M}\right)-\left(\frac{\lambda R_2}{2\pi M}\right)\nabla\left(A_0^2\nabla\phi\left(\frac{\boldsymbol{r}}{M}\right)\right)\right\}$. The first term $A_0^2\left(\frac{\boldsymbol{r}}{M}\right)$ represents x-ray absorption, while for objects mainly composed of light elements, the latter term $\left(\frac{\lambda R_2}{2\pi M}\right)\nabla\left(A_0^2\nabla\phi\left(\frac{\boldsymbol{r}}{M}\right)\right)$ is mainly affected by $\Delta\phi\left(\frac{\boldsymbol{r}}{M}\right)$, which represents the Laplacian of phase changes. We can make the phase contrast image more obvious by increasing λ. However, note that both $A_0^2\left(\frac{\boldsymbol{r}}{M}\right)$ and $\nabla\phi\left(\frac{\boldsymbol{r}}{M}\right)$ are affected by λ, simply decreasing the x-ray photon energy will result in a blurring of both the absorption image and the phase contrast image.

Secondly, consider the incident x-ray intensity $I_{\rm in}$ and the magnification M's influence on the final image's intensity and signal to noise ratio (SNR). It is obvious in the term $\left(\frac{I_{\rm in}}{M^2}\right)$ that a high $I_{\rm in}$ and a small M can result in a strong final image's intensity. Thus, in order to acquire high intensity images, we need to increase the tube current of a microfocus x-ray source and decrease the imaging magnification meanwhile. It should be noted that the tube current does not affect image contrast itself.

Thirdly, we discuss the influence of the focal spot size of x-ray source and the detector. For a microfocus x-ray source, we can assume its focal intensity distribution to be a uniform circle. Using the 2D Fourier transform for a circular focal spot we have [13]

$$\tilde{\mu}_{\rm in}\left(\frac{\lambda R_2\boldsymbol{u}}{M}\right)=\frac{2J_1\left(\pi f(M-1)\left|\boldsymbol{u}\right|/M\right)}{\pi f(M-1)\left|\boldsymbol{u}\right|/M},\quad(10)$$

where f is the diameter of the focal spot and $J_1(x)$ denotes Bessel function of the first kind. Assuming that $M=2$, which is the normal case in in-line imaging, we plot the values of $\tilde{\mu}_{\rm in}\left(\frac{\lambda R_2\boldsymbol{u}}{M}\right)$ in Fig.2 when $f=10\,\mu$m and $f=20\,\mu$m. As the Bessel function $J_1(x)$ gets its first zero point at $x=1.22\pi$, $\tilde{\mu}_{\rm in}\left(\frac{\lambda R_2\boldsymbol{u}}{M}\right)$ gets its first zero point when $\frac{\pi f(M-1)\left|\boldsymbol{u}\right|}{M}=1.22\,\pi$, which means that the limiting resolution determined by the microfocus x-ray source is

$$\boldsymbol{u}_{\rm cut}=\frac{1.22\pi}{\pi f(M-1)/M}=\frac{1.22M}{f(M-1)}.\quad(11)$$

It can be noted from Fig.2 that the smaller the focal spot size, the higher frequency details can we preserve, and thus the more detail can we get in the image.

For a CCD detector, as each pixel is a square shape, we can calculate

$$\mathrm{OTF}_{\rm det}\left(\frac{\boldsymbol{u}}{M}\right)=\sin c\left(\frac{p_{\rm ax}\boldsymbol{u}_x}{M}\right)\sin c\left(\frac{p_{\rm ay}\boldsymbol{u}_y}{M}\right),\quad(12)$$

where $p_{\rm ax}$, $p_{\rm ay}$ are the sizes of a pixel, and $\boldsymbol{u}_x$, $\boldsymbol{u}_y$ are the spatial frequencies in the x and y directions respectively. $\sin c(x)$ gets its first zero point at $x=1$, thus the limiting resolution determined by the CCD detector is

$$\boldsymbol{u}_{x,y}=\frac{M}{p_{\rm ax,ay}}.\quad(13)$$

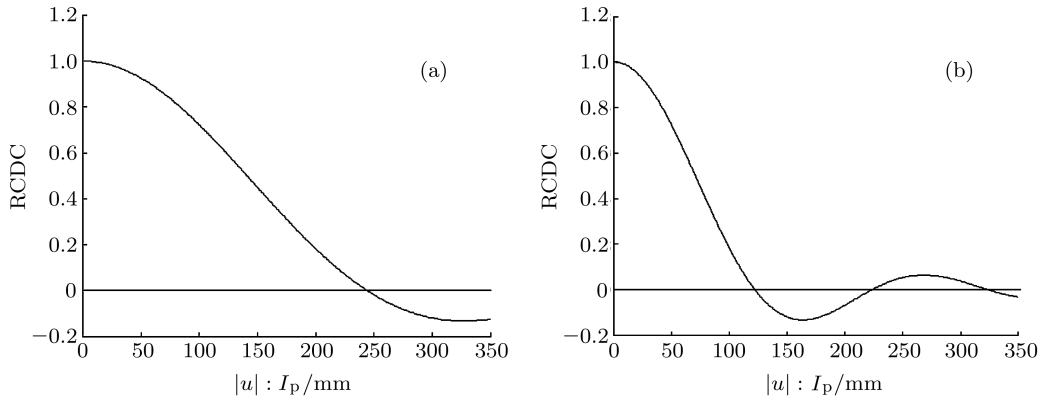


Fig.2. RCDC at $M = 2$ and different focal spot size. (a) $f = 0.01$ mm; (b) $f = 0.02$ mm.

As p_{ax} and p_{ay} decrease, $\mathrm{OTF}_{\mathrm{det}}\left(\frac{\boldsymbol{u}}{M}\right)$ decreases slower with the increase of $\boldsymbol{u}$. Thus, high resolution CCD detector is needed in order to acquire high resolution phase contrast image.

4. Experiment

In-line phase contrast imaging experiments are carried out by using a Feinfocus FXS 160 as the x-ray source. Its maximum tube voltage and current are 160 keV and 3 mA respectively and it has a focal spot whose diameter is 5 μm. We use a Photonic Science X-Ray FDI-2 CCD camera as the detector. It has an active input area of 8.97mm × 6.71mm, and its pixel resolution is set to the optical one which is 6.5 μm × 6.5 μm. The sample is the head of a dried mantis, whose size is about 2 mm × 0.8 mm with a thickness of 0.7 mm around. We hang the sample on a small metal frame, in the middle of which there exists a hole so that x-ray can illuminate the sample without interaction with the frame. As the focal spot, the active input area of the CCD, and the sample are all very small, we hang the sample on the metal frame, and then put it on an automatic carrier to control its position precisely.

Two groups of experiments are conducted at different experimental set. In the first group, we set the object-to-image distance R_2 to 330 mm, the imaging magnification M to 2, and the exposure time to 30 s. Keeping the tube voltage to be 50 keV, we change the tube current from 50 μA to 125 μA with a constant increase of 25 μA, and image the sample at each different tube current. The second group is the same as the first group in all the settings except that the tube current is fixed to 100 μA and the tube voltage is changed from 20 keV to 70 keV. An absorption image is also taken for comparison.

5. Results and discussion

The aim of the first group of experiments is to find out the influence of the tube current. As is discussed earlier in this paper, higher tube current results in higher incident x-ray intensity I_{in}, and will in turn result in higher image intensity. Image intensity as well as the signal-to-noise ratio (SNR) at four different tube currents are calculated and plotted in Fig.3. Here we use average pixel intensity to denote image intensity for convenience.

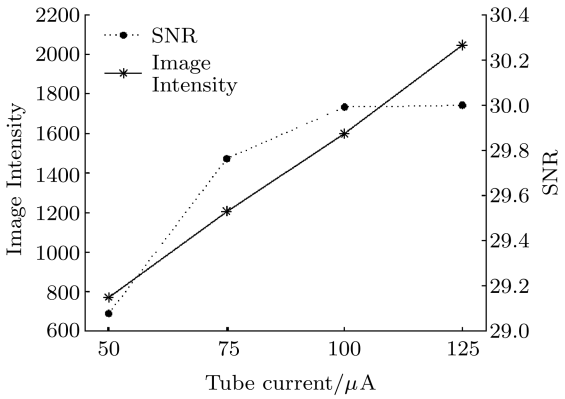


Fig.3. Image intensity and SNR with tube currents of 50 μA, 75 μA, 100 μA, 125 μA, and with a tube voltage of 50keV, $R_2 = 330$ mm, and $M = 2$.

We find in Fig.3 that the intensity of the image is in direct ratio with the increase of tube current. The SNR of the image shows an increase with the augment of tube current, but this increase is so small that it can be ignored.

In the second group of experiments, the tube current is set to 100 μA, and the tube voltage is changed from 20 keV to 70 keV with a constant increase of 10 keV. There are several indices which can evaluate the quality of phase contrast image quantitatively, such as edge-enhanced index,[14] and edge-contrast index (ECI)[15]. We choose ECI as the measurement of our image, for there are lot of details in the imaged mantis. It is calculated by $C = \frac{I_{\text{out}} - I_{\text{in}}}{I_{\text{out}}}$. We calculated and compared the ECIs of several parts of the image. The parts chosen are zoomed out in Fig.4, and the average ECI of the images taken at different tube voltages are depicted in Fig.6. In order to compare the detail-imaging ability of phase contrast imaging with traditional absorption imaging, an absorption image taken at the same tube voltage and current is displayed in Fig.5.

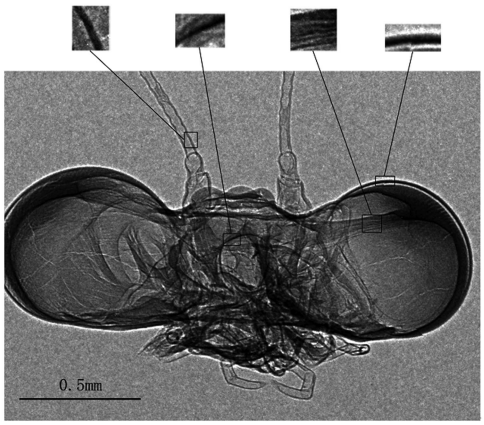


Fig.4. An image of the head of a mantis taken at a tube voltage of 50 keV. Three parts are chosen to calculate ECI: the edge of one eye, the edge of an antenna, and the mid of the head. A part inside one eye is zoomed out to show the tiniest detail of the image. A spatial resolution of 5 μm is achieved.

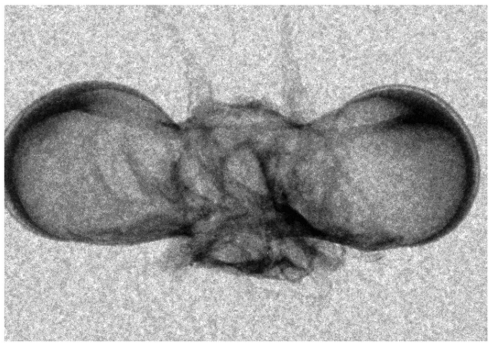


Fig.5. An absorption image taken at the same tube voltage and current as that in Fig.4.

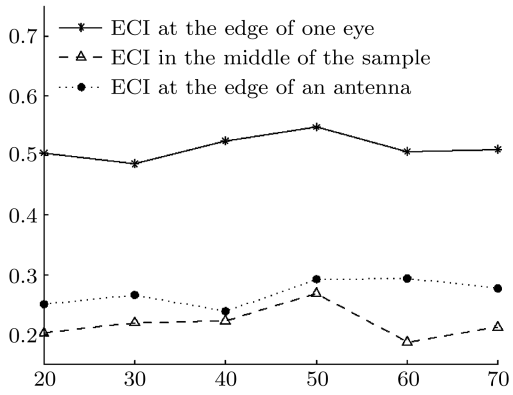


Fig.6. Edge-contrast index of images at different tube voltages. Three parts of the image are compared.

It can be observed that the phase contrast images generally achieve high ECI at a tube voltage around 50 keV. At different positions, images achieve the highest ECI at different tube voltages; this is because of the difference of x-ray phase shift at different parts of the specimen. What's more, the image noise may affect our calculation of ECI, so a fluctuation of the tube voltage where ECI is the highest can be observed. Two factors affect ECI: one is the contrast of phase image to the absorption image, the other one is the intensity of both phase and absorption image. For weakly absorbing tissues, the phase contrast image has far more details than the absorption image. From Eq.(13) we find that the shorter the wave length λ, the higher the contrast of phase image to absorption image. However, x-ray that has long λ will generate phase image and absorption image of low intensity. Thus, only at a moderate wave length, or say, tube voltage, can we acquire phase contrast images of the best quality.

6. Conclusion

In this paper, a comprehensive theory of in-line phase contrast imaging based on Wigner distribution is reviewed. Based on this theory, we analysed the influence of detector and x-ray source on in-line phase contrast imaging. Experiments using a microfocus x-ray source and a high resolution CCD detector are conducted. We find out that the image intensity will increase in direct proportion to tube current, but little increase in SNR will be achieved by modifying the tube current. We also demonstrated that a moderate tube current can help to acquire images of high edge-contrast. By making a comparison between the phase contrast image and the absorption image, strong

detail-imaging ability of in-line phase contrast imaging is evidenced.

Although a spatial resolution of 5μm is achieved in our work, the exposure time of 30 seconds is employed to make sure of high SNR. Such a long exposure time is an obstacle in putting in-line phase contrast imaging into clinical application and computer tomography use. Further work needs to be done on the influence of exposure time on image and we will focus on methods to reduce exposure time in the future.

References

[1] Momose A and Fukuda J 1995 *Med. Phys.* **22** 375

[2] Momose A 1995 *Nucl. Instrum. Methods Phys. Res.* A **353** 622

[3] Davis T J, Gao D, Gurevev T E, Stevenson A W and Wilkins S W 1995 *Nature* **373** 595

[4] Ingral V N and Beliaevskaya E A 1995 *J. Phys.* D **28** 2314

[5] Pogany A, Gao D and Wilkins S 1997 *Rev. Sci. Instrum.* **68** 2774

[6] Zhu H F, Xie H L, Gao H Y, Chen J W, Li R X and Xu Z Z 2004 *Chin. Phys.* **14** 797

[7] Wu X and Liu H 2004 *Med. Phys.* **31** 2378

[8] Wigner E 1932 *Phys. Rev.* **40** 749

[9] Bastiaans M J 1978 *Opt. Commun.* **25** 26

[10] Littlejohn 1986 *Phys. Rep.* **138** 193

[11] Born M and Wolf E 1980 *Principles of Optics* 6th ed (Oxford: Pergamon) p508

[12] Wu X and Liu H 2005 *Applied Optics* **44** 5847

[13] Bracewell R 1986 *The Fourier Transform and Its Applications* 2nd ed (New York: McGraw-Hill) p276

[14] Donnelly E F and Price R R 2002 *Med. Phys.* **29** 999

[15] Zhang D, Li Z, Huang Z F, Yu A M and Sha W 2006 *Chin. Phys.* **15** 1371